Synthesis and gas sensing properties of amorphous NiTiO$_3$

Tianqing Cai[a,b], **Rabigul Tursun**[a,b,*], **Zhaofeng Wu**[a,b], **Qihua Sun**[a,b]

[a] Xinjiang Key Laboratory of Solid State Physics and Devices, Xin Jiang University, Urumqi 830017 China
[b] School of Physical Science and Technology, Xin Jiang University, Urumqi 830017 China

*Corresponding author, e-mail: rabigul@xju.edu.cn

ABSTRACT: Amorphous NiTiO$_3$ nanoparticles were synthesized using the hydrothermal method. The morphology, structure, and gas sensing performance of synthesized NiTiO$_3$ samples were investigated. The analysis's results showed that the synthesized NiTiO$_3$ has an amorphous phase. The amorphous NiTiO$_3$ has no gas sensitivity to ethanol (C$_2$H$_5$OH), benzoic acid (C$_3$H$_6$COOH), or acetone (C$_3$H$_6$O); but it has gas sensitivity to ammonia (NH$_3$), phenol (C$_6$H$_5$OH), formaldehyde (HCHO), water vapor (RH85%), and hydrogen peroxide (H$_2$O$_2$). Due to the anisotropy of the sample phase, NiTiO$_3$ shows higher sensitivity and faster response for multiple target gas analytes. These results show that amorphous NiTiO$_3$ can be used to develop gas sensors.

KEYWORDS: gas sensing performance, NiTiO$_3$, amorphous, material characterization, hydrothermal synthesis

INTRODUCTION

Controlling and monitoring toxic, inflammable, and explosive gases; such as formaldehyde (CH$_2$O), ethanol (C$_2$H$_6$O), and hydrogen peroxide (H$_2$O$_2$); are important for industrial production, indoor life, and public safety. Among diverse types of gas sensors, metal oxide-based gas sensors stand out due to their high sensitivity, rapid response, and stability [1].

Metal titanate oxides, such as ATiO$_3$ (A = Ni, Pb, Fe, Co, Mn, Cu, and Zn) are universally known as inorganic functional materials with many applications such as electrodes for solid oxide fuel cells, metal-air barriers, gas sensors, solid lubricants, and high-performance catalysts [2]. Nickel titanate (NiTiO$_3$), being an important member of the ATiO$_3$ family, has been attracting much attention in recent years because it holds tremendous promises for a wide range of applications, and especially for semiconductor rectifiers, gas sensors, and photocatalysts [3].

To date, solid-state [4], polymer-pyrolysis [5], sol–gel [6], coprecipitation [7], and stearic acid methods [8] have been used to synthesize NiTiO$_3$ powder. The solid phase method is simple to prepare and inexpensive, but it consumes large amounts of energy and has low preparation purity, large particle size, and easy agglomeration. As such, the solid phase method cannot meet industrial requirements. The sol–gel method yields crystals with smaller particle diameter and higher purity, but it produces NO$_2$ pollution caused by the use of nitrates and allows for little control of material morphology [9]. However, no relative experiment synthesis using hydrothermal method has been reported.

To the best of our knowledge, most previous studies on NiTiO$_3$ have mostly focused on its photoluminescence, catalysts, and magnetic properties [10], but very few on amorphous phase synthesis and gas sensing properties analysis. Francioso et al [11] reported that TiO$_2$ nanowire arrays have been synthesized on silicon dioxide, which have good sensitivity to 2% and 3% ethanol at 550 °C. Wilson et al [12] synthesized different thicknesses (8 to 21 nm) of NiO films by chemical vapour deposition. Samples showed promising selective sensitivity towards NO$_2$.

In this study, amorphous phase NiTiO$_3$ was synthesized using the hydrothermal method. The synthesized NiTiO$_3$ samples were studied by X-ray diffraction (XRD), scanning electron microscopy (SEM), high resolution transmission electron microscopy (HRTEM), energy dispersive X-ray spectroscopy (EDS), Raman spectroscopy (Raman), and Fourier transform infrared spectroscopy (FT-IR) using an electrochemical workstation. This paper was the first to report the hydrothermal synthesis of amorphous phase NiTiO$_3$ and its gas sensing properties.

MATERIALS AND METHODS

Materials preparation

NiTiO$_3$ samples were synthesized by hydrothermal method. First, stoichiometric amounts of metal nitrate precursor were dissolved in ethanol and ethylene glycol by magnetic stirring for 30 min. A green transparent solution of Ni^{2+} with a concentration of 0.2 mol/l and a light yellow transparent solution of Ti^{4+} with a concentration of 0.5 mol/l were synthesized. Then citric acid with molar ratio of Ni + Ti 1:1 was added to inhibit the hydrolysis of tetrabutyl titanate. The solution was stirred for 3 h, supplemented with sodium hydroxide to adjust the pH value to 9, transferred to hydrothermal reactor vessel, and then reacted at 200 °C for 18 h. The NiTiO$_3$ samples were obtained.

Material characterization methods

The synthesized $NiTiO_3$ samples were subjected to various characterizations including XRD, EDS, FE-SEM, TEM, RAMAN, FT-IR, and gas-sensing performance. The powder samples were characterized by XRD at room temperature using a Bruker D8 advance (Germany) diffractometer with Cu Kα radiation (λ = 1.5406 Å) at a scanning rate of 8 deg/min in the 2θ range of 20–80°. Analysis of material elements by EDS (SU8010, Japan). FE-SEM (SU8010, Japan) was used to observe the samples' micro morphology. High resolution transmission electron microscopy (HRTEM, JAPAN JEOL-JEM 2100 F, Japan) was used to study the crystal structure and electron diffraction pattern. The $NiTiO_3$ sample structure bonding was characterized by Raman spectroscopy (HR EVLUTION, France) over a measurement range of 50–1200 nm. The FT-IR (VERTEX 70 RAMI, Germany) spectrum of the $NiTiO_3$ sample in a KBr pellet was recorded in the range of 400–4000 cm^{-1}.

Measurement of sensing parameters

The synthesized $NiTiO_3$ sample was dispersed and stirred and in deionized water to form a paste. The paste was, then, dropped onto an interdigital electrode sheet; and the sheet, after static drying, was put into a gas sensing test device. The gas-sensing performance of the samples was tested at room temperature using an electrochemical workstation (CIMPS-2, ZAHER EN-NIUM, Beijing, China). A constant potential of 4 V was applied across the sensor, and the relative change of electric current when switching from air to the target gases was recorded by an electrochemical workstation at room temperature. The response was defined as: response $= \Delta I / I_R = (I_R - I_G)/I_R$, where I_R and I_G were electric currents in the reference gas and the target gas, respectively. The response time of the gas sensor is the time required for the resistance value to reach 90% of the maximum in the target gas, and the recovery time is the time required for the resistance value to reach 10% [13].

RESULTS AND DISCUSSION

XRD analysis

Fig. 1(a) displays the XRD pattern of synthesized $NiTiO_3$ samples reacted at 200 °C for 18 h. The XRD pattern was composed of only broad maxima without any diffraction peaks reflecting crystallite, indicating the amorphous nature within the resolution of XRD. HR-TEM (High Resolution Transmission Electron Microscope) images were taken to characterize the morphology of $NiTiO_3$ at very high spatial resolution. Consistently, electron diffraction pattern Fig. 1(b) displays broad rings, which is typical for amorphous materials. These results were in agreement with those obtained using XRD analysis. Fig. 1(c) shows a structure with
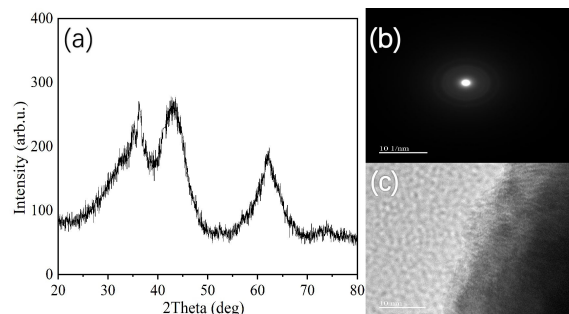
Fig. 1 (a), XRD pattern of $NiTiO_3$ samples; (b), Electron diffraction pattern; (c), HRTEM image.
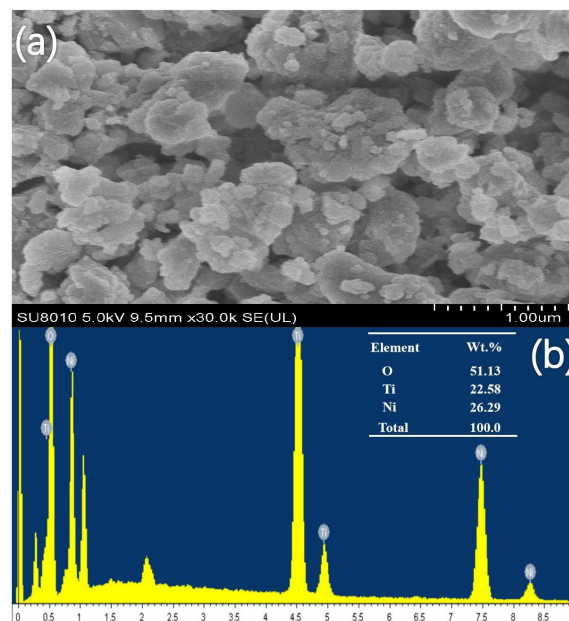
Fig. 2 (a), FE-SEM image of $NiTiO_3$ samples synthesized at 200 °C for 18 h; (b), EDS analysis of $NiTiO_3$ samples. Insets indicate the amount of elements.

no long-range order, a characteristic of an amorphous structure.

Morphology analysis

Fig. 2(a) shows SEM images of the $NiTiO_3$ pigments obtained at 200 °C. The sample had no obvious shapes or an uneven distribution of features. EDS (Energy-dispersive X-ray spectroscopy) was used to further confirm the composition of the obtained samples. The EDS analysis of the obtained products (Fig. 2(b)) indicated that samples were composed of titanium, nickel, oxygen, and small amount of carbon with an approximate molar ratio of Ni:Ti:O of 1:1:3. Other peaks were due to instrumental effects and were not marked.
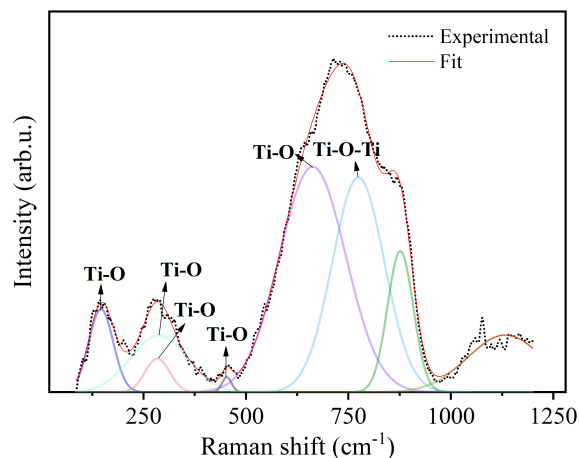
Fig. 3 Raman spectra of NiTiO$_3$ samples synthesized at 200 °C.

Fig. 4 FT-IR spectra of NiTiO$_3$ samples synthesized at 200 °C.

Raman spectrum analysis

The room temperature Raman spectra in the range of 50–1200 cm^{-1} for the NiTiO$_3$ samples were shown in Fig. 3. Due to the weak Raman modes, peak broadening was observed. Lorentzian line shape least squares fitting was used to fit the Raman spectra to determine peak positions. Eight active Raman modes were identified (Fig. 3).

The Raman peak at 146.1 cm^{-1} could be attributed to the symmetric stretching vibrations of Ti—O. The Raman modes at 283.7 cm^{-1} and 287.1 cm^{-1} could be attributed to the twist of the oxygen octahedral due to the vibrations of the Ni and Ti atoms parallel to the XY plane [14]. The vibrational peaks at 453.1 and 662.6 cm^{-1} could be attributed to the asymmetric breathing of the oxygen octahedral and twist with the cationic vibrations parallel to the XY plane [14]. The peaks observed at 774.2 cm^{-1} corresponded to Ti—O bond stretching vibrations in the TiO$_6$ octahedral. Additional Raman peaks were observed at 876.5 cm^{-1} and 1132.6 cm^{-1}; and they were shoulder peaks to the Raman mode at 774.2 cm^{-1}. These shoulder peaks (876.5 cm^{-1}, and 1132.6 cm^{-1}) were not a fundamental Raman mode, and they could be attributed to the fractional amorphous content of the samples, with their broad appearance [15]. The presence of this 283.1 cm^{-1} peak indicates the possible presence of TiO$_2$ in our material [16].

FT-IR analysis

The FT-IR spectra of the KBr mixed pellets were recorded across a wavelength range of 400–4000 cm^{-1}. In the FT-IR spectra, six major absorption bands were observed, and their positions in terms of frequency (cm^{-1}) were presented in Fig. 4. The broad absorption band around 3199.43 cm^{-1} could be attributed to the stretching vibration of a

hydroxyl group (—OH). The peaks at 1635.25 and 1486.09 cm^{-1} were due to the N—O bond vibration of NO$_3^-$ and carboxyl vibration, respectively. The strong band at 1360.39 cm^{-1} could be attributed to the symmetric mode. The bands appeared 1058.39 cm^{-1} possibilities were due to the stretching vibration of C—O [17]. The bands in the low-wavelength region (400–650 cm^{-1}) could be attributed to Ti—O bond vibrations [18].

Gas sensitivity analysis

Next, we examined the gas sensing performance of our nickel titanate material. The selectivity of a gas sensor is the ability to sense a specific target gas, producing a response significantly higher than that of other gases. Fig. 5 shows the selectivity of the NiTiO$_3$ sensor to 1000 ppm concentrations of ammonia (NH$_3$), phenol (C$_6$H$_5$OH), formaldehyde (HCHO), water vapor (RH85%), hydrogen peroxide (H$_2$O$_2$), ethanol (C$_2$H$_5$OH), benzoic acid (C$_3$H$_6$COOH), and acetone (C$_3$H$_6$O) at room temperature. It could be inferred from the graph (Fig. 5) that selectivity of the sensor to C$_2$H$_5$OH, C$_3$H$_6$COOH, and C$_3$H$_6$O was poor; and selectivity to NH$_3$, C$_6$H$_5$OH, HCHO, RH85%, and H$_2$O$_2$ was good. As shown in Fig. 5, NiTiO$_3$ detected three consecutive peaks of the target gas, showing good repeatability [19]; and the corresponding current change graph was shown in Fig. 6. In order to further comprehensively evaluate the sensing performance, the average response results were shown in Fig. 7. The response rates to 1000 ppm concentrations of ammonia, phenol, formaldehyde, water vapor, and hydrogen peroxide were 25230%, 10168%, 13800%, 9731%, and 10181%, respectively. Therefore, gas sensing performance was stable. The high selectivity of NiTiO$_3$ to NH$_3$ might be due to the existence of a
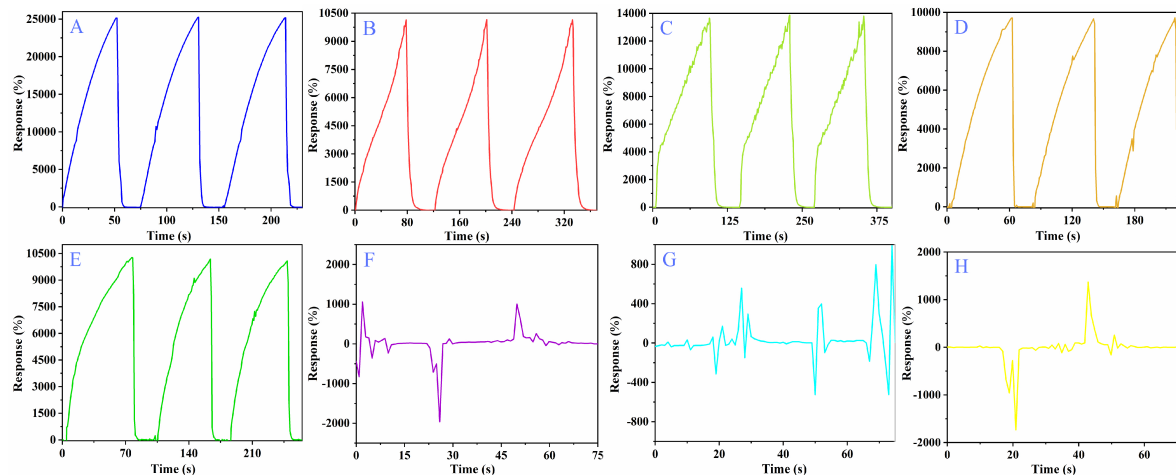
Fig. 5 Dynamic sensing curves of NiTiO$_3$ samples to 1000 ppm of: A, (NH$_3$); B, (C$_6$H$_5$OH); C, (HCHO); D, (RH); E, (H$_2$O$_2$); F, (C$_3$H$_6$O); G, (C$_2$H$_5$OH); and H, (C$_3$H$_6$COOH).
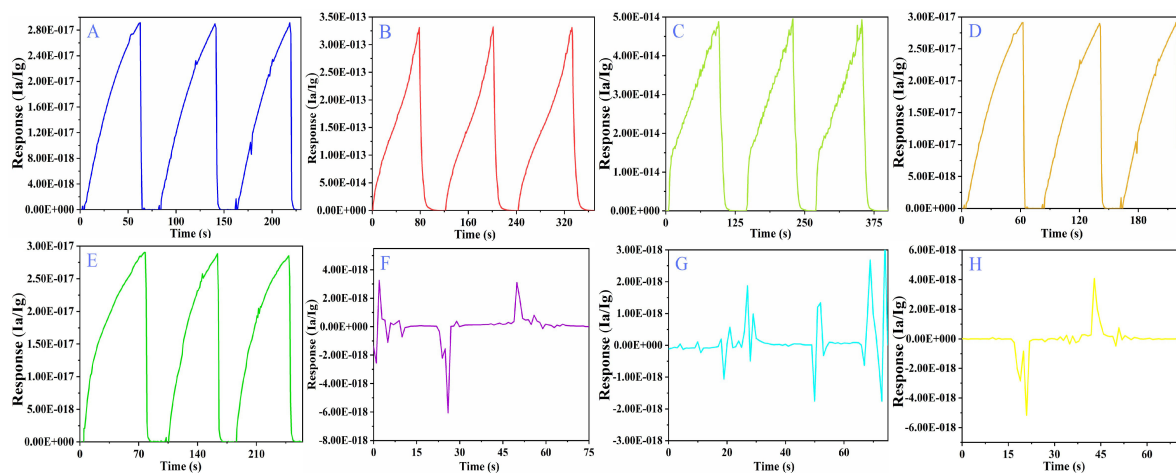
Fig. 6 The dynamic response curves (Ia/Ig) and response time of NiTiO$_3$ to 1000 ppm of: A, (NH$_3$); B, (C$_6$H$_5$OH); C, (HCHO); D, (RH); E, (H$_2$O$_2$); F, (C$_3$H$_6$O); G, (C$_2$H$_5$OH); and H, (C$_3$H$_6$COOH).

small amount of TiO$_2$ in the material. Furthermore, in many experiments, besides the higher affinity of NH$_3$ to TiO$_2$, the presence of TiO$_2$ might be beneficial to improve the sensitivity of the gas sensor [20].

Sensing properties of NiTiO$_3$

NiTiO$_3$ is an n-type semiconductor mainly composed of electrons as carriers, based on the modulation of the loss layer by oxygen absorption (Fig. 8). Oxygen from the atmosphere captures electrons from the NiTiO$_3$ conduction band, and positive ions are left. These immobile positive ions form a space charge layer near the surface of the sensor and cause a bent band. Below 147 °C, oxygen is adsorbed as O$_2^-$. Between 147 °C and 397 °C, which are mainly the working temperatures of the gas sensors, oxygen is adsorbed as O$^-$. Above 397 °C, O$_2^-$ is formed. Take NH$_3$ as an

example, when NH$_3$ is contacted, O$_2^-$ reacts with NH$_3$ molecules, providing electrons to NiTiO$_3$, reducing the depletion layer width and resistance of the NiTiO$_3$ sensor (Fig. 7). According to literature reports [21], the possible gas-sensing mechanism is as follows:

$$2NH_3 + 3O_2^-(ads) \longrightarrow 2H_2O + 2N_2 + 6e^- \quad (1)$$
$$2NH_3 + 2O_2^-(ads) \longrightarrow H_2O + N_2O + 2e^- \quad (2)$$
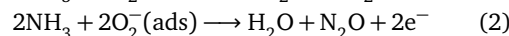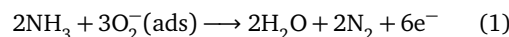
CONCLUSION

In this study, amorphous phase NiTiO$_3$ was synthesized at 200 °C for 18 h using the hydrothermal method. Morphology, microstructure, and gas sensing properties of the NiTiO$_3$ samples were then studied. XRD, EDSiijŇSEM and HR-TEM, Raman, and FT-IR analyses showed that the NiTiO$_3$ samples have an amorphous structure. Analysis of gas sensing performance showed
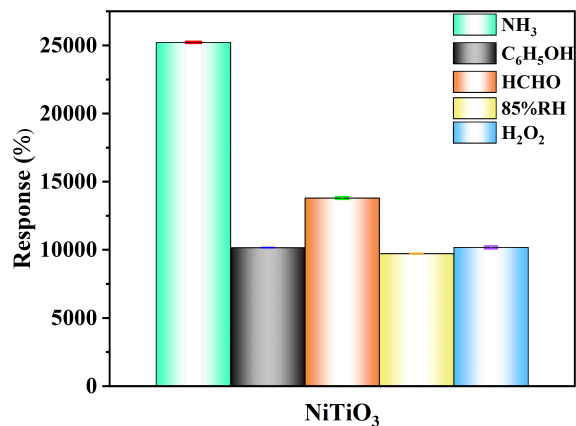
Fig. 7 The selectivity of $NiTiO_3$ gas sensor to various gases of 1000 ppm concentration.
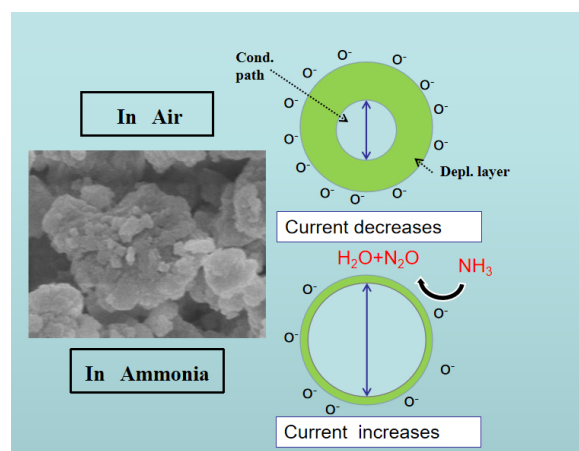
Fig. 8 Proposed mechanism for NH_3 sensing using $NiTiO_3$ sensor.

that amorphous $NiTiO_3$ sensor has no gas sensitivity to C_2H_5OH, C_3H_6COOH, C_3H_6O, but has gas sensitivity to NH_3, C_6H_5OH, HCHO, RH85%, and H_2O_2. The capacity of $NiTiO_3$ for gas sensing could be attributed to the anisotropy of amorphous phase. These results showed that amorphous $NiTiO_3$ could be used to develop gas sensors. This study provided an important guidance for the synthesis of new amorphous materials and the design of room temperature sensors.

REFERENCES

1. Long H, Zeng W, Zhang H (2015) Synthesis of WO_3 and its gas sensing: A review. *J Mater Sci Mater Electron* **26**, 4698–4707.

2. Ruiz-Preciado MA, Kassiba A, Gibaud A, Morales-Acevedo A (2015) Comparison of nickel titanate ($NiTiO_3$) powders synthesized by sol–gel and solid state reaction. *Mater Sci Semicond Process* **37**, 171–178.

3. Li T, Wang CC, Lei CM, Sun XH, Wang GJ, Liu LN (2013) Conductivity relaxation in $NiTiO_3$ at high temperatures. *Current Applied Physics* **13**, 1728–1731.

4. Henkes AE, Bauer JC, Sra AK, Johnson RD, Cable RE, Schaak RE (2005) Low-temperature nanoparticle-directed solid-state synthesis of ternary and quaternary transition metal oxides. *Chem Mater* **18**, 567–571.

5. Lopes KP, Cavalcante LS, Simões AZ, Varela JA, Longo E, Leite ER (2009) $NiTiO_3$ powders obtained by polymeric precursor method: Synthesis and characterization. *J Alloys Compd* **468**, 327–332.

6. Della Gaspera E, Pujatti M, Guglielmi M, Post ML, Martucci A (2011) Structural evolution and hydrogen sulfide sensing properties of $NiTiO_3$-TiO_2 sol–gel thin films containing Au nanoparticles. *Mater Sci Eng B* **176**, 716–722.

7. Murugan AV, Samuel V, Navale SC, Ravi V (2006) Phase evolution of $NiTiO_3$ synthesized by coprecipitation method. *Mater Lett* **60**, 1791–1792.

8. Sadjadi MS, Zare K, Khanahmadzadeh S, Enhessari M (2008) Structural characterization of $NiTiO_3$ nanopowders synthesized by stearic acid gel method. *Mater Lett* **62**, 3679–3681.

9. Mi L, Zhang Q, Wang H, Wu Z, Guo Y, Li Y, Xiong X, Liu K, et al (2020) Synthesis of $BaTiO_3$ nanoparticles by sol–gel assisted solid phase method and its formation mechanism and photocatalytic activity. *Ceram Int* **46**, 10619–10633.

10. Tursun R, Su Y, Yu Q, Tan J (2018) Room-temperature coexistence of electric and magnetic orders in $NiTiO_3$ and effect of ethylene glycol. *Mater Sci Eng B* **228**, 96–102.

11. Francioso L, Taurino A, Forleo A, Siciliano P (2008) TiO_2 nanowires array fabrication and gas sensing properties. *Sens Actuators B* **130**, 70–76.

12. Wilson RL, Simion CE, Stanoiu A, Taylor A, Guldin S, Covington JA, Carmalt CJ, Blackman CS (2020) Humidity-tolerant ultrathin NiO gas-sensing films. *ACS Sens* **5**, 1389–1397.

13. Chaudhari P, Mishra S (2017) Ilmenite phase nickel titanate nanowhiskers as highly sensitive LPG sensor at room temperature. *J Mater Sci Mater Electron* **29**, 117–123.

14. Chellasamy V, Thangadurai P (2017) Structural and electrochemical investigations of nanostructured $NiTiO_3$ in acidic environment. *Front Mater Sci* **11**, 162–170.

15. Ruiz-Preciado MA, Bulou A, Makowska-Janusik M, Gibaud A, Morales-Acevedo A, Kassiba A (2016) Nickel titanate ($NiTiO_3$) thin films: RF-sputtering synthesis and investigation of related features for photocatalysis. *CrystEngComm* **18**, 3229–3236.

16. Busca G, Ramis G, Amores JMG, Escribano VS, Piaggio P (1994) FT Raman and FTIR studies of titanias and metatitanate powders. *J Chem Soc Faraday Trans* **90**, 3181–3190.

17. Fei LM (2011) Synthesis and infrared spectroscopy characterization of organosilicone modified polyurethanes. *Technological Pioneers* **4**, 185–186.

18. Gambhire AB, Lande MK, Kalokhe SB, Mandale AB, Patil KR, Gholap RS, Arbad BR (2008) Synthesis and characterizations of NiTiO$_3$ nanoparticles synthesized by the sol–gel process. *Philos Mag Lett* **88**, 467–472.
19. Dey A (2018) Semiconductor metal oxide gas sensors: A review. *Mater Sci Eng B* **229**, 206–217.
20. Chen Y, Wu J, Xu Z, Shen W, Wu Y, Corriou J-P (2022) Computational assisted tuning of Co-doped TiO$_2$ nanoparticles for ammonia detection at room temperatures. *Appl Surf Sci* **601**, 154214.
21. Huang J, Jiang D, Zhou J, Ye J, Sun Y, Li X, Geng Y, Wang J, et al (2021) Visible light-activated room temperature NH3 sensor base on CuPc-loaded ZnO nanorods. *Sens Actuators B* **327**, 128911.